



First observation of the decay $\bar{B}_s^0 \rightarrow D^0 K^{*0}$ and a measurement of the ratio of branching fractions

$$\frac{\mathcal{B}(\bar{B}_s^0 \rightarrow D^0 K^{*0})}{\mathcal{B}(\bar{B}^0 \rightarrow D^0 \rho^0)}$$

Submitted to Phys. Lett. B

The LHCb Collaboration ¹

Abstract

The first observation of the decay $\bar{B}_s^0 \rightarrow D^0 K^{*0}$ using pp data collected by the LHCb detector at a centre-of-mass energy of 7 TeV, corresponding to an integrated luminosity of 36 pb^{-1} , is reported. A signal of 34.4 ± 6.8 events is obtained and the absence of signal is rejected with a statistical significance of more than nine standard deviations. The $\bar{B}_s^0 \rightarrow D^0 K^{*0}$ branching fraction is measured relative to that of $\bar{B}^0 \rightarrow D^0 \rho^0$: $\frac{\mathcal{B}(\bar{B}_s^0 \rightarrow D^0 K^{*0})}{\mathcal{B}(\bar{B}^0 \rightarrow D^0 \rho^0)} = 1.48 \pm 0.34 \pm 0.15 \pm 0.12$, where the first uncertainty is statistical, the second systematic and the third is due to the uncertainty on the ratio of the B^0 and B_s^0 hadronisation fractions.

¹Authors are listed on the following pages.

The LHCb Collaboration

R. Aaij²³, C. Abellan Beteta^{35,n}, B. Adeva³⁶, M. Adinolfi⁴², C. Adrover⁶, A. Affolder⁴⁸, Z. Ajaltouni⁵, J. Albrecht³⁷, F. Alessio³⁷, M. Alexander⁴⁷, G. Alkhazov²⁹, P. Alvarez Cartelle³⁶, A.A. Alves Jr²², S. Amato², Y. Amhis³⁸, J. Anderson³⁹, R.B. Appleby⁵⁰, O. Aquines Gutierrez¹⁰, F. Archilli^{18,37}, L. Arrabito⁵³, A. Artamonov³⁴, M. Artuso^{52,37}, E. Aslanides⁶, G. Auriemma^{22,m}, S. Bachmann¹¹, J.J. Back⁴⁴, D.S. Bailey⁵⁰, V. Balagura^{30,37}, W. Baldini¹⁶, R.J. Barlow⁵⁰, C. Barschel³⁷, S. Barsuk⁷, W. Barter⁴³, A. Bates⁴⁷, C. Bauer¹⁰, Th. Bauer²³, A. Bay³⁸, I. Bediaga¹, K. Belous³⁴, I. Belyaev^{30,37}, E. Ben-Haim⁸, M. Benayoun⁸, G. Bencivenni¹⁸, S. Benson⁴⁶, J. Benton⁴², R. Bernet³⁹, M.-O. Bettler¹⁷, M. van Beuzekom²³, A. Bien¹¹, S. Bifani¹², A. Bizzeti^{17,h}, P.M. Bjørnstad⁵⁰, T. Blake⁴⁹, F. Blanc³⁸, C. Blanks⁴⁹, J. Blouw¹¹, S. Blusk⁵², A. Bobrov³³, V. Bocci²², A. Bondar³³, N. Bondar²⁹, W. Bonivento¹⁵, S. Borghi⁴⁷, A. Borgia⁵², T.J.V. Bowcock⁴⁸, C. Bozzi¹⁶, T. Brambach⁹, J. van den Brand²⁴, J. Bressieux³⁸, D. Brett⁵⁰, S. Brisbane⁵¹, M. Britsch¹⁰, T. Britton⁵², N.H. Brook⁴², H. Brown⁴⁸, A. Büchler-Germann³⁹, I. Burducea²⁸, A. Bursche³⁹, J. Buytaert³⁷, S. Cadeddu¹⁵, J.M. Caicedo Carvajal³⁷, O. Callot⁷, M. Calvi^{20,j}, M. Calvo Gomez^{35,n}, A. Camboni³⁵, P. Campana^{18,37}, A. Carbone¹⁴, G. Carboni^{21,k}, R. Cardinale^{19,i,37}, A. Cardini¹⁵, L. Carson³⁶, K. Carvalho Akiba²³, G. Casse⁴⁸, M. Cattaneo³⁷, M. Charles⁵¹, Ph. Charpentier³⁷, N. Chiapolini³⁹, K. Ciba³⁷, X. Cid Vidal³⁶, G. Ciezarek⁴⁹, P.E.L. Clarke^{46,37}, M. Clemencic³⁷, H.V. Cliff⁴³, J. Closier³⁷, C. Coca²⁸, V. Coco²³, J. Cogan⁶, P. Collins³⁷, A. Comerma-Montells³⁵, F. Constantin²⁸, G. Conti³⁸, A. Contu⁵¹, A. Cook⁴², M. Coombes⁴², G. Corti³⁷, G.A. Cowan³⁸, R. Currie⁴⁶, B. D'Almagne⁷, C. D'Ambrosio³⁷, P. David⁸, I. De Bonis⁴, S. De Capua^{21,k}, M. De Cian³⁹, F. De Lorenzi¹², J.M. De Miranda¹, L. De Paula², P. De Simone¹⁸, D. Decamp⁴, M. Deckenhoff⁹, H. Degaudenzi^{38,37}, M. Deissenroth¹¹, L. Del Buono⁸, C. Deplano¹⁵, O. Deschamps⁵, F. Dettori^{15,d}, J. Dickens⁴³, H. Dijkstra³⁷, P. Diniz Batista¹, F. Domingo Bonal^{35,n}, S. Donleavy⁴⁸, A. Dosil Suárez³⁶, D. Dossett⁴⁴, A. Dovbnya⁴⁰, F. Dupertuis³⁸, R. Dzhelyadin³⁴, S. Easo⁴⁵, U. Egede⁴⁹, V. Egorychev³⁰, S. Eidelman³³, D. van Eijk²³, F. Eisele¹¹, S. Eisenhardt⁴⁶, R. Ekelhof⁹, L. Eklund⁴⁷, Ch. Elsasser³⁹, D.G. d'Enterria^{35,o}, D. Esperante Pereira³⁶, L. Estève⁴³, A. Falabella^{16,e}, E. Fanchini^{20,j}, C. Färber¹¹, G. Fardell⁴⁶, C. Farinelli²³, S. Farry¹², V. Fave³⁸, V. Fernandez Albor³⁶, M. Ferro-Luzzi³⁷, S. Filippov³², C. Fitzpatrick⁴⁶, M. Fontana¹⁰, F. Fontanelli^{19,i}, R. Forty³⁷, M. Frank³⁷, C. Frei³⁷, M. Frosini^{17,f,37}, S. Furcas²⁰, A. Gallas Torreira³⁶, D. Galli^{14,c}, M. Gandelman², P. Gandini⁵¹, Y. Gao³, J.-C. Garnier³⁷, J. Garofoli⁵², J. Garra Tico⁴³, L. Garrido³⁵, D. Gascon³⁵, C. Gaspar³⁷, N. Gauvin³⁸, M. Gersabeck³⁷, T. Gershon^{44,37}, Ph. Ghez⁴, V. Gibson⁴³, V.V. Gligorov³⁷, C. Göbel⁵⁴, D. Golubkov³⁰, A. Golutvin^{49,30,37}, A. Gomes², H. Gordon⁵¹, M. Grabalosa Gándara³⁵, R. Graciani Diaz³⁵, L.A. Granado Cardoso³⁷, E. Graugés³⁵, G. Graziani¹⁷, A. Grecu²⁸, E. Greening⁵¹, S. Gregson⁴³, B. Gui⁵², E. Gushchin³², Yu. Guz³⁴, T. Gys³⁷, G. Haefeli³⁸, C. Haen³⁷, S.C. Haines⁴³, T. Hampson⁴², S. Hansmann-Menzemer¹¹, R. Harji⁴⁹, N. Harnew⁵¹, J. Harrison⁵⁰, P.F. Harrison⁴⁴, J. He⁷, V. Heijne²³, K. Hennessy⁴⁸, P. Henrard⁵, J.A. Hernando Morata³⁶, E. van Herwijnen³⁷, E. Hicks⁴⁸, W. Hofmann¹⁰, K. Holubyev¹¹, P. Hopchev⁴, W. Hulsbergen²³, P. Hunt⁵¹, T. Huse⁴⁸, R.S. Huston¹², D. Hutchcroft⁴⁸, D. Hynds⁴⁷, V. Iakovenko⁴¹, P. Ilten¹², J. Imong⁴², R. Jacobsson³⁷, A. Jaeger¹¹, M. Jahjah Hussein⁵, E. Jans²³, F. Jansen²³, P. Jaton³⁸, B. Jean-Marie⁷, F. Jing³, M. John⁵¹,

D. Johnson⁵¹, C.R. Jones⁴³, B. Jost³⁷, S. Kandybei⁴⁰, M. Karacson³⁷, T.M. Karbach⁹,
 J. Keaveney¹², U. Kerzel³⁷, T. Ketel²⁴, A. Keune³⁸, B. Khanji⁶, Y.M. Kim⁴⁶, M. Knecht³⁸,
 S. Koblitz³⁷, P. Koppenburg²³, A. Kozlinskiy²³, L. Kravchuk³², K. Kreplin¹¹, M. Kreps⁴⁴,
 G. Krocker¹¹, P. Krokovny¹¹, F. Kruse⁹, K. Kruzelecki³⁷, M. Kucharczyk^{20,25,37}, S. Kukulak²⁵,
 R. Kumar^{14,37}, T. Kvaratskheliya^{30,37}, V.N. La Thi³⁸, D. Lacarrere³⁷, G. Lafferty⁵⁰, A. Lai¹⁵,
 D. Lambert⁴⁶, R.W. Lambert³⁷, E. Lanciotti³⁷, G. Lanfranchi¹⁸, C. Langenbruch¹¹,
 T. Latham⁴⁴, R. Le Gac⁶, J. van Leerdam²³, J.-P. Lees⁴, R. Lefèvre⁵, A. Leflat^{31,37},
 J. Lefrancois⁷, O. Leroy⁶, T. Lesiak²⁵, L. Li³, L. Li Gioi⁵, M. Lieng⁹, M. Liles⁴⁸, R. Lindner³⁷,
 C. Linn¹¹, B. Liu³, G. Liu³⁷, J.H. Lopes², E. Lopez Asamar³⁵, N. Lopez-March³⁸, J. Luisier³⁸,
 F. Machefert⁷, I.V. Machikhiliyan^{4,30}, F. Maciuc¹⁰, O. Maev^{29,37}, J. Magnin¹, S. Malde⁵¹,
 R.M.D. Mamunur³⁷, G. Manca^{15,d}, G. Mancinelli⁶, N. Mangiafave⁴³, U. Marconi¹⁴,
 R. Märki³⁸, J. Marks¹¹, G. Martellotti²², A. Martens⁷, L. Martin⁵¹, A. Martín Sánchez⁷,
 D. Martinez Santos³⁷, A. Massafferri¹, Z. Mathe¹², C. Matteuzzi²⁰, M. Matveev²⁹, E. Maurice⁶,
 B. Maynard⁵², A. Mazurov^{16,32,37}, G. McGregor⁵⁰, R. McNulty¹², C. Mclean¹⁴, M. Meissner¹¹,
 M. Merk²³, J. Merkel⁹, R. Messi^{21,k}, S. Miglioranzi³⁷, D.A. Milanes^{13,37}, M.-N. Minard⁴,
 S. Monteil⁵, D. Moran¹², P. Morawski²⁵, R. Mountain⁵², I. Mous²³, F. Muheim⁴⁶, K. Müller³⁹,
 R. Muresan^{28,38}, B. Muryn²⁶, M. Musy³⁵, J. Mylroie-Smith⁴⁸, P. Naik⁴², T. Nakada³⁸,
 R. Nandakumar⁴⁵, J. Nardulli⁴⁵, I. Nasteva¹, M. Nedos⁹, M. Needham⁴⁶, N. Neufeld³⁷,
 C. Nguyen-Mau^{38,p}, M. Nicol⁷, S. Nies⁹, V. Niess⁵, N. Nikitin³¹, A. Nomerotski⁵¹,
 A. Oblakowska-Mucha²⁶, V. Obraztsov³⁴, S. Oggero²³, S. Ogilvy⁴⁷, O. Okhrimenko⁴¹,
 R. Oldeman^{15,d}, M. Orlandea²⁸, J.M. Otalora Goicochea², P. Owen⁴⁹, K. Pal⁵², J. Palacios³⁹,
 A. Palano^{13,b}, M. Palutan¹⁸, J. Panman³⁷, A. Papanestis⁴⁵, M. Pappagallo^{13,b}, C. Parkes^{47,37},
 C.J. Parkinson⁴⁹, G. Passaleva¹⁷, G.D. Patel⁴⁸, M. Patel⁴⁹, S.K. Paterson⁴⁹, G.N. Patrick⁴⁵,
 C. Patrignani^{19,i}, C. Pavel-Nicorescu²⁸, A. Pazos Alvarez³⁶, A. Pellegrino²³, G. Penso^{22,l},
 M. Pepe Altarelli³⁷, S. Perazzini^{14,c}, D.L. Perego^{20,j}, E. Perez Trigo³⁶,
 A. Pérez-Calero Yzquierdo³⁵, P. Perret⁵, M. Perrin-Terrin⁶, G. Pessina²⁰, A. Petrella^{16,37},
 A. Petrolini^{19,i}, E. Picatoste Olloqui³⁵, B. Pie Valls³⁵, B. Pietrzyk⁴, T. Pilar⁴⁴, D. Pinci²²,
 R. Plackett⁴⁷, S. Playfer⁴⁶, M. Plo Casasus³⁶, G. Polok²⁵, A. Poluektov^{44,33}, E. Polycarpo²,
 D. Popov¹⁰, B. Popovici²⁸, C. Potterat³⁵, A. Powell⁵¹, T. du Pree²³, J. Prisciandaro³⁸,
 V. Pugatch⁴¹, A. Puig Navarro³⁵, W. Qian⁵², J.H. Rademacker⁴², B. Rakotomiaramanana³⁸,
 M.S. Rangel², I. Raniuk⁴⁰, G. Raven²⁴, S. Redford⁵¹, M.M. Reid⁴⁴, A.C. dos Reis¹,
 S. Ricciardi⁴⁵, K. Rinnert⁴⁸, D.A. Roa Romero⁵, P. Robbe⁷, E. Rodrigues⁴⁷, F. Rodrigues²,
 P. Rodriguez Perez³⁶, G.J. Rogers⁴³, S. Roiser³⁷, V. Romanovsky³⁴, M. Rosello^{35,n},
 J. Rouvinet³⁸, T. Ruf³⁷, H. Ruiz³⁵, G. Sabatino^{21,k}, J.J. Saborido Silva³⁶, N. Sagidova²⁹,
 P. Sail⁴⁷, B. Saitta^{15,d}, C. Salzmann³⁹, M. Sannino^{19,i}, R. Santacesaria²², R. Santinelli³⁷,
 E. Santovetti^{21,k}, M. Sapunov⁶, A. Sarti^{18,l}, C. Satriano^{22,m}, A. Satta²¹, M. Savrie^{16,e},
 D. Savrina³⁰, P. Schaack⁴⁹, M. Schiller¹¹, S. Schleich⁹, M. Schmelling¹⁰, B. Schmidt³⁷,
 O. Schneider³⁸, A. Schopper³⁷, M.-H. Schune⁷, R. Schwemmer³⁷, B. Sciascia¹⁸, A. Sciubba^{18,l},
 M. Seco³⁶, A. Semennikov³⁰, K. Senderowska²⁶, I. Sepp⁴⁹, N. Serra³⁹, J. Serrano⁶, P. Seyfert¹¹,
 B. Shao³, M. Shapkin³⁴, I. Shapoval^{40,37}, P. Shatalov³⁰, Y. Shcheglov²⁹, T. Shears⁴⁸,
 L. Shekhtman³³, O. Shevchenko⁴⁰, V. Shevchenko³⁰, A. Shires⁴⁹, R. Silva Coutinho⁵⁴,
 H.P. Skottowe⁴³, T. Skwarnicki⁵², A.C. Smith³⁷, N.A. Smith⁴⁸, E. Smith^{51,45}, K. Sobczak⁵,
 F.J.P. Soler⁴⁷, A. Solomin⁴², F. Soomro⁴⁹, B. Souza De Paula², B. Spaan⁹, A. Sparkes⁴⁶,
 P. Spradlin⁴⁷, F. Stagni³⁷, S. Stahl¹¹, O. Steinkamp³⁹, S. Stoica²⁸, S. Stone^{52,37}, B. Storaci²³,
 M. Straticiu²⁸, U. Straumann³⁹, N. Styles⁴⁶, V.K. Subbiah³⁷, S. Swientek⁹, M. Szczekowski²⁷,
 P. Szczypka³⁸, T. Szumlak²⁶, S. T'Jampens⁴, E. Teodorescu²⁸, F. Teubert³⁷, C. Thomas^{51,45},

E. Thomas³⁷, J. van Tilburg¹¹, V. Tisserand⁴, M. Tobin³⁹, S. Topp-Joergensen⁵¹, N. Torri⁵¹, M.T. Tran³⁸, A. Tsaregorodtsev⁶, N. Tuning²³, A. Ukleja²⁷, P. Urquijo⁵², U. Uwer¹¹, V. Vagnoni¹⁴, G. Valenti¹⁴, R. Vazquez Gomez³⁵, P. Vazquez Regueiro³⁶, S. Vecchi¹⁶, J.J. Velthuis⁴², M. Veltri^{17,g}, K. Vervink³⁷, B. Viaud⁷, I. Videau⁷, X. Vilasis-Cardona^{35,n}, J. Visniakov³⁶, A. Vollhardt³⁹, D. Voong⁴², A. Vorobyev²⁹, H. Voss¹⁰, K. Wacker⁹, S. Wandernoth¹¹, J. Wang⁵², D.R. Ward⁴³, A.D. Webber⁵⁰, D. Websdale⁴⁹, M. Whitehead⁴⁴, D. Wiedner¹¹, L. Wiggers²³, G. Wilkinson⁵¹, M.P. Williams^{44,45}, M. Williams⁴⁹, F.F. Wilson⁴⁵, J. Wishahi⁹, M. Witek²⁵, W. Witzeling³⁷, S.A. Wotton⁴³, K. Wyllie³⁷, Y. Xie⁴⁶, F. Xing⁵¹, Z. Xing⁵², Z. Yang³, R. Young⁴⁶, O. Yushchenko³⁴, M. Zavertyaev^{10,a}, L. Zhang⁵², W.C. Zhang¹², Y. Zhang³, A. Zhelezov¹¹, L. Zhong³, E. Zverev³¹, A. Zvyagin³⁷.

¹Centro Brasileiro de Pesquisas Físicas (CBPF), Rio de Janeiro, Brazil

²Universidade Federal do Rio de Janeiro (UFRJ), Rio de Janeiro, Brazil

³Center for High Energy Physics, Tsinghua University, Beijing, China

⁴LAPP, Université de Savoie, CNRS/IN2P3, Annecy-Le-Vieux, France

⁵Clermont Université, Université Blaise Pascal, CNRS/IN2P3, LPC, Clermont-Ferrand, France

⁶CPPM, Aix-Marseille Université, CNRS/IN2P3, Marseille, France

⁷LAL, Université Paris-Sud, CNRS/IN2P3, Orsay, France

⁸LPNHE, Université Pierre et Marie Curie, Université Paris Diderot, CNRS/IN2P3, Paris, France

⁹Fakultät Physik, Technische Universität Dortmund, Dortmund, Germany

¹⁰Max-Planck-Institut für Kernphysik (MPIK), Heidelberg, Germany

¹¹Physikalisches Institut, Ruprecht-Karls-Universität Heidelberg, Heidelberg, Germany

¹²School of Physics, University College Dublin, Dublin, Ireland

¹³Sezione INFN di Bari, Bari, Italy

¹⁴Sezione INFN di Bologna, Bologna, Italy

¹⁵Sezione INFN di Cagliari, Cagliari, Italy

¹⁶Sezione INFN di Ferrara, Ferrara, Italy

¹⁷Sezione INFN di Firenze, Firenze, Italy

¹⁸Laboratori Nazionali dell'INFN di Frascati, Frascati, Italy

¹⁹Sezione INFN di Genova, Genova, Italy

²⁰Sezione INFN di Milano Bicocca, Milano, Italy

²¹Sezione INFN di Roma Tor Vergata, Roma, Italy

²²Sezione INFN di Roma La Sapienza, Roma, Italy

²³Nikhef National Institute for Subatomic Physics, Amsterdam, Netherlands

²⁴Nikhef National Institute for Subatomic Physics and Vrije Universiteit, Amsterdam, Netherlands

²⁵Henryk Niewodniczanski Institute of Nuclear Physics Polish Academy of Sciences, Cracow, Poland

²⁶Faculty of Physics & Applied Computer Science, Cracow, Poland

²⁷Soltan Institute for Nuclear Studies, Warsaw, Poland

²⁸Horia Hulubei National Institute of Physics and Nuclear Engineering, Bucharest-Magurele, Romania

²⁹Petersburg Nuclear Physics Institute (PNPI), Gatchina, Russia

³⁰Institute of Theoretical and Experimental Physics (ITEP), Moscow, Russia

³¹Institute of Nuclear Physics, Moscow State University (SINP MSU), Moscow, Russia

³²Institute for Nuclear Research of the Russian Academy of Sciences (INR RAN), Moscow, Russia

³³Budker Institute of Nuclear Physics (SB RAS) and Novosibirsk State University, Novosibirsk, Russia

³⁴Institute for High Energy Physics (IHEP), Protvino, Russia

³⁵Universitat de Barcelona, Barcelona, Spain

³⁶Universidad de Santiago de Compostela, Santiago de Compostela, Spain

³⁷European Organization for Nuclear Research (CERN), Geneva, Switzerland

³⁸Ecole Polytechnique Fédérale de Lausanne (EPFL), Lausanne, Switzerland

³⁹Physik-Institut, Universität Zürich, Zürich, Switzerland

⁴⁰NSC Kharkiv Institute of Physics and Technology (NSC KIPT), Kharkiv, Ukraine

- ⁴¹*Institute for Nuclear Research of the National Academy of Sciences (KINR), Kyiv, Ukraine*
- ⁴²*H.H. Wills Physics Laboratory, University of Bristol, Bristol, United Kingdom*
- ⁴³*Cavendish Laboratory, University of Cambridge, Cambridge, United Kingdom*
- ⁴⁴*Department of Physics, University of Warwick, Coventry, United Kingdom*
- ⁴⁵*STFC Rutherford Appleton Laboratory, Didcot, United Kingdom*
- ⁴⁶*School of Physics and Astronomy, University of Edinburgh, Edinburgh, United Kingdom*
- ⁴⁷*School of Physics and Astronomy, University of Glasgow, Glasgow, United Kingdom*
- ⁴⁸*Oliver Lodge Laboratory, University of Liverpool, Liverpool, United Kingdom*
- ⁴⁹*Imperial College London, London, United Kingdom*
- ⁵⁰*School of Physics and Astronomy, University of Manchester, Manchester, United Kingdom*
- ⁵¹*Department of Physics, University of Oxford, Oxford, United Kingdom*
- ⁵²*Syracuse University, Syracuse, NY, United States*
- ⁵³*CC-IN2P3, CNRS/IN2P3, Lyon-Villeurbanne, France, associated member*
- ⁵⁴*Pontifícia Universidade Católica do Rio de Janeiro (PUC-Rio), Rio de Janeiro, Brazil, associated to ²*
- ^a*P.N. Lebedev Physical Institute, Russian Academy of Science (LPI RAS), Moscow, Russia*
- ^b*Università di Bari, Bari, Italy*
- ^c*Università di Bologna, Bologna, Italy*
- ^d*Università di Cagliari, Cagliari, Italy*
- ^e*Università di Ferrara, Ferrara, Italy*
- ^f*Università di Firenze, Firenze, Italy*
- ^g*Università di Urbino, Urbino, Italy*
- ^h*Università di Modena e Reggio Emilia, Modena, Italy*
- ⁱ*Università di Genova, Genova, Italy*
- ^j*Università di Milano Bicocca, Milano, Italy*
- ^k*Università di Roma Tor Vergata, Roma, Italy*
- ^l*Università di Roma La Sapienza, Roma, Italy*
- ^m*Università della Basilicata, Potenza, Italy*
- ⁿ*LIFAELS, La Salle, Universitat Ramon Llull, Barcelona, Spain*
- ^o*Institució Catalana de Recerca i Estudis Avançats (ICREA), Barcelona, Spain*
- ^p*Hanoi University of Science, Hanoi, Viet Nam*

1 Introduction

A theoretically clean extraction of the Cabibbo-Kobayashi-Maskawa (CKM) unitarity triangle angle γ can be performed using time-integrated $B \rightarrow DX$ decays by exploiting the interference between Cabibbo-suppressed $b \rightarrow u$ and Cabibbo-allowed $b \rightarrow c$ transitions [1, 2, 3, 4, 5, 6]. One of the most promising channels for this purpose is $\bar{B}^0 \rightarrow D\bar{K}^{*0}$, where D represents a D^0 or a \bar{D}^0 meson.² Although this channel involves the decay of a neutral B meson, the final state is self-tagged by the flavour of the K^{*0} so that a time-dependent analysis is not required. In the $\bar{B}^0 \rightarrow D\bar{K}^{*0}$ decay, both the $\bar{B}^0 \rightarrow D^0\bar{K}^{*0}$ and the $\bar{B}^0 \rightarrow \bar{D}^0\bar{K}^{*0}$ are colour suppressed. Therefore, although the $\bar{B}^0 \rightarrow D\bar{K}^{*0}$ decay has a lower branching fraction compared to the $B^+ \rightarrow DK^+$ mode, it could exhibit an enhanced interference.

The Cabibbo-allowed $\bar{B}_s^0 \rightarrow D^0K^{*0}$ and $\bar{B}_s^0 \rightarrow D^{*0}K^{*0}$ decays potentially provide a significant background to the Cabibbo-suppressed $\bar{B}^0 \rightarrow \bar{D}^0\bar{K}^{*0}$ decay. The expected size of this background is unknown, since the $\bar{B}_s^0 \rightarrow D^{(*)0}K^{*0}$ decay has not yet been observed. In addition, a measurement of the branching fraction of $\bar{B}_s^0 \rightarrow D^0K^{*0}$ is of interest as a probe of SU(3) breaking in colour suppressed $\bar{B}_{(d,s)}^0 \rightarrow D^0V$ decays [7, 8], where V denotes a neutral vector meson. Thus, the detailed study of $\bar{B}_s^0 \rightarrow D^0K^{*0}$ is an important goal with the first LHCb data.

The LHCb detector [9] is a forward spectrometer constructed to measure decays of hadrons containing b and c quarks. The detector elements, placed along the collision axis of the Large Hadron Collider (LHC), start with the Vertex Locator, a silicon strip device that surrounds the pp interaction region with its innermost sensitive part positioned 8 mm from the beam. It precisely determines the locations of the primary pp interaction vertices, the locations of the decay vertices of long-lived hadrons, and contributes to the measurement of track momenta. Other tracking detectors include a large-area silicon strip detector located upstream of the 4 Tm dipole magnet and a combination of silicon strip detectors and straw drift chambers placed downstream. Two Ring-Imaging Cherenkov (RICH) detectors are used to identify charged hadrons. Further downstream an electromagnetic calorimeter is used for photon detection and electron identification, followed by a hadron calorimeter and a muon system consisting of alternating layers of iron and gaseous chambers. LHCb operates a two stage trigger system. In the first stage hardware trigger the rate is reduced from the visible interaction rate to about 1 MHz using information from the calorimeters and muon system. In the second stage software trigger the rate is further reduced to 2 kHz by performing a set of channel specific selections based upon a full event reconstruction. During the 2010 data taking period, several trigger configurations were used for both stages in order to cope with the varying beam conditions.

The results reported here uses 36 pb⁻¹ of pp data collected at the LHC at a centre-of-mass energy $\sqrt{s} = 7$ TeV in 2010. The strategy of the analysis is to measure a ratio of branching fractions in which most of the potentially large systematic uncertainties

²In this Letter the mention of a decay will refer also to its charge-conjugate state.

cancel. The decay $\bar{B}^0 \rightarrow D^0 \rho^0$ is used as the normalisation channel. In both decay channels, the D^0 is reconstructed in the Cabibbo-allowed decay mode $D^0 \rightarrow K^- \pi^+$; the contribution from the doubly Cabibbo-suppressed $D^0 \rightarrow K^+ \pi^-$ decay is negligible. The K^{*0} is reconstructed in the $K^{*0} \rightarrow K^+ \pi^-$ decay mode and the ρ^0 in the $\rho^0 \rightarrow \pi^+ \pi^-$ decay mode. The main systematic uncertainties arise from the different particle identification requirements and the pollution of the $\bar{B}^0 \rightarrow D^0 \rho^0$ peak by $\bar{B}^0 \rightarrow D^0 \pi^+ \pi^-$ decays where the $\pi^+ \pi^-$ pairs do not originate from a ρ^0 resonance. In addition, the normalisation of the B_s^0 decay to a B^0 decay suffers from a systematic uncertainty of 8 % due to the current knowledge of the ratio of the fragmentation fractions $f_s/f_d = 0.267_{-0.020}^{+0.021}$ [10].

2 Events selection

Monte Carlo samples of signal and background events are used to optimize the signal selection and to parametrize the probability density functions (PDFs) used in the fit. Proton beam collisions are generated with PYTHIA [11] and decays of hadronic particles are provided by EvtGen [12]. The generated particles are traced through the detector with GEANT4 [13], taking into account the details of the geometry and material composition of the detector.

B^0 and B_s^0 mesons are reconstructed from a selected D^0 meson combined with a vector particle (ρ^0 or K^{*0}). The selection requirements are kept as similar as possible for $\bar{B}_s^0 \rightarrow D^0 K^{*0}$ and $\bar{B}^0 \rightarrow D^0 \rho^0$. The four charged particles in the decay are each required to have a transverse momentum $p_T > 300$ MeV/ c for the daughters of the vector particle and $p_T > 250$ MeV/ c (400 MeV/ c) for the pion (kaon) from the D^0 meson decay. The χ^2 of the track impact parameter with respect to any primary vertex is required to be greater than 4. A cut on the absolute value of the cosine of the helicity angle of the vector meson greater than 0.4 is applied. The tracks of the D^0 meson daughters are combined to form a vertex with a goodness of fit χ^2/ndf smaller than 5. The B meson vertex formed by the D^0 and the tracks of the V meson daughters is required to satisfy $\chi^2/\text{ndf} < 4$. The smallest impact parameter of the B meson with respect to all the primary vertices is required to be smaller than 9 and defines uniquely the primary vertex associated to the B meson. Since the B^0 or B_s^0 should point towards the primary vertex, the angle between the B momentum and the B line of flight defined by the line between the B vertex and the primary vertex is required to be less than 10 mrad. Finally, since the measured z position (along the beam direction) of the D vertex (z_D) is not expected to be situated significantly upstream of the z position of the vector particle vertex (z_V), a requirement of $(z_D - z_V)/\sqrt{\sigma_{z,D}^2 + \sigma_{z,V}^2} > -2$ is applied, where $\sigma_{z,D}$ and $\sigma_{z,V}$ are the uncertainties on the z positions of the D and V vertices respectively.

The selection criteria for the V candidates introduce some differences between the signal and normalisation channel due to the particle identification (PID) and mass window requirements. The K^{*0} (ρ^0) reconstructed mass is required to be within 50 MeV/ c^2 (150 MeV/ c^2) of its nominal value [14]. The selection criteria for the D^0 and vector mesons include identifying kaon and pion candidates using the RICH system. This analysis uses

the comparison between the kaon and pion hypotheses, $\text{DLL}_{K\pi}$, which represents the difference in logarithms of likelihoods for the K with respect to the π hypothesis. The particle identification requirements for both kaon and pion hypotheses have been optimized on data. The thresholds are set at $\text{DLL}_{K\pi} > 0$ and $\text{DLL}_{K\pi} < 4$, respectively, for the kaon and the pion from the D^0 . The misidentification rate is kept low by setting the thresholds for the vector meson daughters to $\text{DLL}_{K\pi} > 3$ and $\text{DLL}_{K\pi} < 3$ for the kaon and pion respectively. In order to remove the potential backgrounds due to $\bar{B}_s^0 \rightarrow D_s^+ \pi^-$ and $\bar{B}^0 \rightarrow D^+ \pi^-$ with $D_s^- \rightarrow K^{*0} K^-$ and $D^- \rightarrow K^{*0} K^-$, vetoes around the nominal D^- and D_s^- meson masses [14] of $\pm 15 \text{ MeV}/c^2$ are applied. Monte Carlo studies suggest that these vetoes are more than 99.5% efficient on the signal.

Finally, multiple candidates in an event (about 5%) are removed by choosing the B candidate with the largest B flight distance significance and which lies in the mass windows of the D^0 and the vector meson resonance.

3 Extraction of the ratio of branching fractions

The ratio of branching fractions is calculated from the number of signal events in the two decay channels $\bar{B}_s^0 \rightarrow D^0 K^{*0}$ and $\bar{B}^0 \rightarrow D^0 \rho^0$,

$$\frac{\mathcal{B}(\bar{B}_s^0 \rightarrow D^0 K^{*0})}{\mathcal{B}(\bar{B}^0 \rightarrow D^0 \rho^0)} = \frac{N_{\bar{B}_s^0 \rightarrow D^0 K^{*0}}^{\text{sig.}}}{N_{\bar{B}^0 \rightarrow D^0 \rho^0}^{\text{sig.}}} \times \frac{\mathcal{B}(\rho^0 \rightarrow \pi^+ \pi^-)}{\mathcal{B}(K^{*0} \rightarrow K^+ \pi^-)} \times \frac{f_d}{f_s} \times \frac{\epsilon_{\bar{B}^0 \rightarrow D^0 \rho^0}}{\epsilon_{\bar{B}_s^0 \rightarrow D^0 K^{*0}}} \quad (1)$$

where the ϵ parameters represent the total efficiencies, including acceptance, trigger, reconstruction and selection, and f_s/f_d is the ratio of B^0 and B_s^0 hadronization fractions in pp collisions at $\sqrt{s} = 7 \text{ TeV}$. Since a given event can either be triggered by tracks from the signal or by tracks from the other B hadron decay, absolute efficiencies cannot be obtained with a great precision from the Monte Carlo simulation due to improper modelling of the generic B hadron decays. In order to reduce the systematic uncertainty related to the Monte Carlo simulation of the trigger, the data sample is divided into two categories: candidates that satisfy only the hadronic hardware trigger³ (**TOSonly**, since they are Triggered On the Signal (TOS) exclusively and not on the rest of the event) and events which are Triggered by the rest of the event Independent of the Signal candidate B decay (**TIS**). Approximately 6% of candidates do not enter either of these two categories, and are vetoed in the analysis. The $\bar{B}^0 \rightarrow D^0 \rho^0$ signal yield is extracted separately for the two trigger categories **TOSonly** and **TIS**; the $\bar{B}_s^0 \rightarrow D^0 K^{*0}$ signal yield is extracted from the sum of both data samples. The ratio of efficiencies are sub-divided into the contributions arising from the selection requirements (including acceptance effects, but excluding PID), r_{sel} , the PID requirements, r_{PID} , and the trigger requirements, r_{TOSonly}

³Events passing only the muon trigger on the signal candidate tracks are rejected.

and r_{TIS} . The ratio of the branching fractions can therefore be expressed as

$$\frac{\mathcal{B}(\bar{B}_s^0 \rightarrow D^0 K^{*0})}{\mathcal{B}(\bar{B}^0 \rightarrow D^0 \rho^0)} = \frac{\mathcal{B}(\rho^0 \rightarrow \pi^+ \pi^-)}{\mathcal{B}(K^{*0} \rightarrow K^+ \pi^-)} \times \frac{f_d}{f_s} \times r_{\text{sel}} \times r_{\text{PID}} \times \frac{N_{\bar{B}_s^0 \rightarrow D^0 K^{*0}}^{\text{sig.}}}{\alpha \left(\frac{N_{\bar{B}^0 \rightarrow D^0 \rho^0}^{\text{TOSonly}}}{r_{\text{TOSonly}}} + \frac{N_{\bar{B}^0 \rightarrow D^0 \rho^0}^{\text{TIS}}}{r_{\text{TIS}}} \right)}, \quad (2)$$

where α represents a correction factor for the “non- ρ^0 ” contribution in the $\bar{B}^0 \rightarrow D^0 \rho^0$ decays.

The values of the efficiency ratios are measured using simulated events, except for $r_{\text{PID}} = 1.09 \pm 0.08$ which is obtained from data using the $D^* \rightarrow D^0 \pi$ decay with $D^0 \rightarrow K^- \pi^+$ where clean samples of kaons and pions can be obtained using a purely kinematic selection. Since the event selection is identical for the D^0 in the two channels of interest, many factors cancel out in $r_{\text{sel}} = 0.784 \pm 0.024$ thereby reducing the systematic uncertainties. The values of the trigger efficiency ratios, $r_{\text{TOSonly}} = 1.20 \pm 0.08$ and $r_{\text{TIS}} = 1.03 \pm 0.03$, depend on the trigger configurations and are therefore computed from a luminosity-weighted average. The quoted uncertainties reflect the difference between data and Monte Carlo simulation mainly caused by the energy calibration of the trigger.

The numbers of events in the two $D^0 \rho^0$ trigger categories, $N_{\bar{B}^0 \rightarrow D^0 \rho^0}^{\text{TOSonly}}$ and $N_{\bar{B}^0 \rightarrow D^0 \rho^0}^{\text{TIS}}$, and $N_{\bar{B}_s^0 \rightarrow D^0 K^{*0}}^{\text{sig.}}$ are extracted from a simultaneous unbinned maximum likelihood fit to the data. In order to simplify the description of the partially reconstructed background, the lower edge of the B meson mass window is restricted to $5.1 \text{ GeV}/c^2$ for the $\bar{B}^0 \rightarrow D^0 \rho^0$ decay mode and to $5.19 \text{ GeV}/c^2$ for the $\bar{B}_s^0 \rightarrow D^0 K^{*0}$ decay mode. There are four types of events in each category: signal, combinatorial background, partially reconstructed background and cross-feed.⁴ The signal B meson mass PDFs for $\bar{B}^0 \rightarrow D^0 \rho^0$ and $\bar{B}_s^0 \rightarrow D^0 K^{*0}$ are parametrized for each channel using the sum of two Gaussians sharing the same mean value. The mean and width of the core Gaussian describing the $\bar{B}^0 \rightarrow D^0 \rho^0$ mass distribution are allowed to vary in the fit. The fraction of events in the core Gaussian, 0.81 ± 0.02 , and the ratio of the tail and core Gaussian widths, 2.04 ± 0.05 , are fixed to the values obtained from Monte Carlo simulation. In order to take into account the difference in mass resolution for the $\bar{B}^0 \rightarrow D^0 \rho^0$ and $\bar{B}_s^0 \rightarrow D^0 K^{*0}$ decay modes, the value of the ratio of core Gaussian widths $\frac{\sigma_{D^0 K^{*0}}}{\sigma_{D^0 \rho^0}} = 0.89 \pm 0.03$ is fixed from the Monte Carlo simulation. The mass difference between the means of the B^0 and B_s^0 signals is fixed to the nominal value [14].

The combinatorial background mass distribution is modelled by a flat PDF and the partially reconstructed background is parametrized by an exponential function; the exponential slope is different in the $\bar{B}^0 \rightarrow D^0 \rho^0$ and $\bar{B}_s^0 \rightarrow D^0 K^{*0}$ categories. Since the number of $\bar{B}^0 \rightarrow D^0 \rho^0$ decays is larger than that of $\bar{B}_s^0 \rightarrow D^0 K^{*0}$, the contribution from misidentified pions as kaons from real $\bar{B}^0 \rightarrow D^0 \rho^0$ has to be taken into account. The fractions of the cross-feed events, $f_{D^0 \rho^0 \rightarrow D^0 K^{*0}} = 0.062 \pm 0.031$ and $f_{D^0 K^{*0} \rightarrow D^0 \rho^0} = 0.095 \pm 0.047$, are

⁴The cross-feed events are due to particle misidentification on one of the vector daughters; some $D^0 \rho^0$ events can be selected as $D^0 K^{*0}$ and vice versa.

constrained using the results from a Monte Carlo study corrected by the PID misidentification rates measured in data. The PDF for the cross-feed is empirically parametrised by a Crystal Ball function [15], whose width and other parameters are taken from a fit to simulated events in which $\bar{B}_s^0 \rightarrow D^0 K^{*0}$ events are misidentified as $\bar{B}^0 \rightarrow D^0 \rho^0$ and vice versa; the width is fixed to 1.75 times the signal resolution. For the $\bar{B}^0 \rightarrow D^0 \rho^0$ decay mode, the events are further split according to the TOSOnly and TIS categories.

In summary, 13 parameters are free in the fit. Four shape parameters are used, two for the signal and two for the partially reconstructed backgrounds. In addition, nine event yields are extracted, three (signal, combinatorial and partially reconstructed backgrounds) in each of the three categories: $\bar{B}^0 \rightarrow D^0 \rho^0$ (TOSOnly and TIS) and $\bar{B}_s^0 \rightarrow D^0 K^{*0}$.

The results of the fit for $D^0 \rho^0$ and $\bar{B}_s^0 \rightarrow D^0 K^{*0}$ are shown in Fig. 1 and Fig. 2. The overall signal yields are 154.1 ± 15.1 and 34.4 ± 6.8 respectively. The yields for the different components are summarised in Table 1.

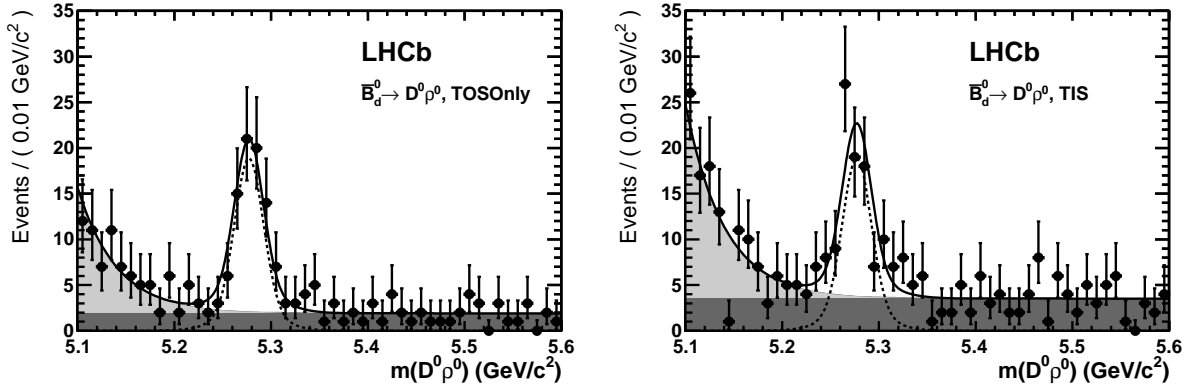


Figure 1: The invariant mass distribution for the $\bar{B}^0 \rightarrow D^0 \rho^0$ decay mode for the TOSOnly (left) and TIS (right) trigger categories with the result of the fit superimposed. The black points correspond to the data and the fit result is represented as a solid line. The signal is fitted with a double Gaussian (dashed line), the partially reconstructed background with an exponential function (light grey area) and the combinatorial background with a flat distribution (dark grey area) as explained in the text. The contributions from cross-feed are too small to be visible.

Table 1: Summary of the fitted yields for the different categories. The background yields are quoted for the full mass regions.

Decay mode	Signal yield	Part. rec. bkgd yield	Comb. bkgd yield
$\bar{B}_s^0 \rightarrow D^0 K^{*0}$	34.4 ± 6.8	17.5 ± 11.4	29.8 ± 8.4
$\bar{B}^0 \rightarrow D^0 \rho^0$ (TOSOnly)	77.0 ± 10.1	55.4 ± 10.1	95.5 ± 13.1
$\bar{B}^0 \rightarrow D^0 \rho^0$ (TIS)	77.1 ± 11.2	85.6 ± 12.9	176.0 ± 17.5

In order to check the existence of other contributions under the vector mass peaks,

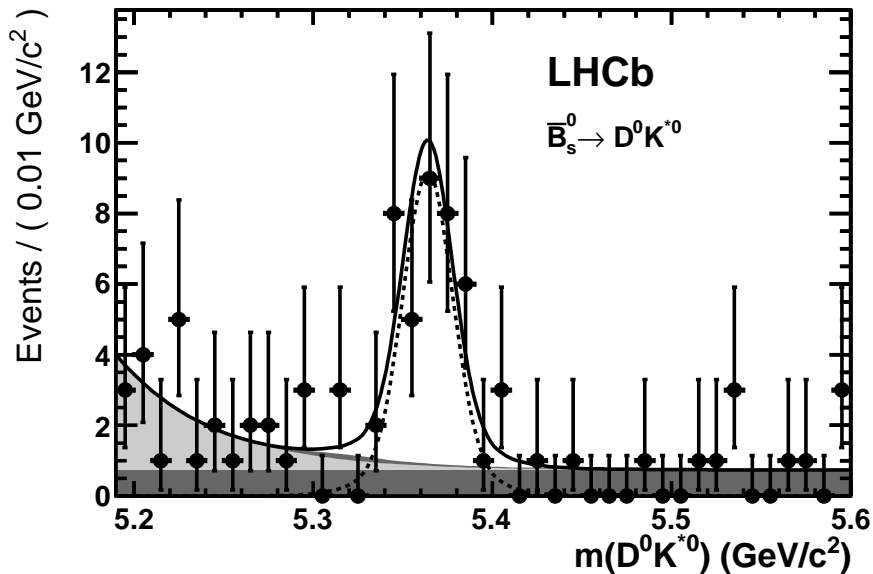


Figure 2: The invariant mass distribution for the $\bar{B}_s^0 \rightarrow D^0 K^{*0}$ decay mode with the result of the fit superimposed. The black points correspond to the data and the fit result is represented as a solid line. The signal is fitted with a double Gaussian (dashed line), the partially reconstructed background with an exponential function (light grey area), the combinatorial background with a flat distribution (dark grey area) and the cross-feed from $\bar{B}^0 \rightarrow D^0 \rho^0$ (intermediate grey area) as explained in the text.

the sPlot technique [16] has been used to obtain background subtracted invariant mass distributions. The sWeights are calculated from the reconstructed B invariant mass distribution using the same parametrization as in the analysis, the selection being the same except for the V invariant mass ranges which are widened. It was checked that there is no correlation between the B and the V invariant mass. The resulting plots are shown in Fig. 3, where the resonant component is fitted with a Breit-Wigner convoluted with a Gaussian and the non-resonant part with a second order polynomial. While the K^{*0} region shows no sign of an extra contribution, the ρ^0 region shows a more complicated structure. An effective “non- ρ^0 ” contribution is estimated using a second-order polynomial: 30.1 ± 7.9 events contribute in the ρ^0 mass window (± 150 MeV/ c^2). The measured $\bar{B}^0 \rightarrow D^0 \rho^0$ yields are corrected by a factor $\alpha = 0.805 \pm 0.054$ (see Eq. 2), consistent with expectations based on previous studies of the $\bar{B}^0 \rightarrow D^0 \pi^+ \pi^-$ Dalitz plot [17, 18].

The ratio of branching fractions, $\frac{\mathcal{B}(\bar{B}_s^0 \rightarrow D^0 K^{*0})}{\mathcal{B}(\bar{B}^0 \rightarrow D^0 \rho^0)}$, is calculated using the measured yields of the $\bar{B}^0 \rightarrow D^0 \rho^0$ signal in the two trigger categories, corrected for the “non- ρ^0 ” events and assumed to contribute proportionally to the TOSonly and TIS samples, the $\bar{B}_s^0 \rightarrow D^0 K^{*0}$ yield and the values of the r ratios quoted above. The result is $\frac{\mathcal{B}(\bar{B}_s^0 \rightarrow D^0 K^{*0})}{\mathcal{B}(\bar{B}^0 \rightarrow D^0 \rho^0)} = 1.48 \pm 0.34$, where the uncertainty is statistical only. The small statistical correlation between the two

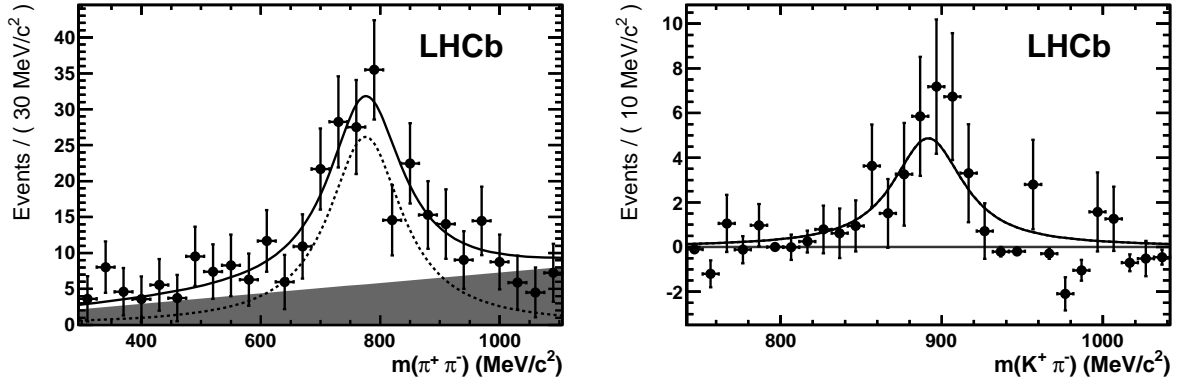


Figure 3: The ρ^0 (on the left) and K^{*0} (on the right) invariant mass distributions obtained from data using an sPlot technique. The level of non K^{*0} combinations in the $\bar{B}_s^0 \rightarrow D^0 K^{*0}$ peak is negligible. Despite being mainly due to $D^0 \rho^0$ combinations, the $\bar{B}^0 \rightarrow D^0 \rho^0$ contains a significant contribution of “non- ρ^0 ” events. The black points correspond to the data and the fit result is represented as a solid line. The resonant component is fitted with a Breit-Wigner convoluted with a Gaussian (dashed line) and the non-resonant part, if present, with a second-order polynomial (grey area).

yields due to the cross-feed has been neglected.

4 Systematic uncertainties

A summary of the contributions to the systematic uncertainty is given in Table 2. The PID performances are determined with a $D^* \rightarrow D^0 \pi$ data calibration sample reweighted according to the kinematical properties of our signals obtained from Monte Carlo simulation. The systematic uncertainty has been assigned using the kinematical distributions directly obtained from the data. However, due to the small signal yield in the B_s^0 case, this systematic uncertainty suffers from large statistical fluctuations which directly translate into a large systematic uncertainty on the kaon identification. The statistical uncertainty obtained on the number of “non- ρ^0 ” events present in the ρ^0 the mass window ($\pm 150 \text{ MeV}/c^2$) has been propagated in the systematic uncertainty. The differences observed between Monte Carlo simulation and data on the values of the D^0 and vector mesons reconstructed masses, as well as on the transverse momentum spectra, have been propagated into the uncertainty quoted on r_{sel} . The relative abundances of TOSonly and TIS triggered events determined from simulated signal are in good agreement with those measured from data. This provides confidence in the description of the trigger in the Monte Carlo simulation. Since these relative abundances are directly measured in data, they do not enter the systematic uncertainty evaluation. However, the difference in trigger efficiency between the $\bar{B}^0 \rightarrow D^0 \rho^0$ and the $\bar{B}_s^0 \rightarrow D^0 K^{*0}$ decay modes is taken from Monte Carlo simulation; this is considered reliable since the difference arises due to the kinematical properties of the decays which are well modelled in the simulation.

The difference in the energy measurement between the hardware trigger clustering and the offline reconstruction clustering is conservatively taken as a systematic uncertainty due to the hadronic trigger threshold. The systematic uncertainty due to the TIS trigger performances on the two decay modes is obtained assuming that it does not depend on the decay mode ($r_{\text{TIS}} = 1$).

The systematic uncertainty due to the PDF parametrizations has been evaluated using toy Monte Carlo simulations where the different types of background have been generated using an alternative parametrization (wide Gaussians for the partially reconstructed backgrounds, first order polynomial for the combinatorial backgrounds) but fitted with the default PDFs.

The total systematic uncertainty is obtained by combining all sources in quadrature. The dominant sources of systematic uncertainty are of statistical nature and will be reduced with more data. The error on the ratio of the fragmentation fractions [10] is quoted as a separate systematic uncertainty.

Table 2: Summary of the contributions to the systematic uncertainties. The uncertainty on the r ratio gives the range used for the systematic uncertainty extraction on the ratios of the branching fractions.

Source	Relative uncertainty
Difference between data and MC to compute $r_{\text{PID}} = 1.09 \pm 0.06$	5.8 %
Uncertainty on the “non- ρ^0 ” component $\alpha = 0.805 \pm 0.054$	6.8 %
MC selection efficiencies $r_{\text{sel.}} = 0.784 \pm 0.024$	3.1 %
L0 Hadron threshold $r_{\text{TOSonly}} = 1.20 \pm 0.08$	3.0 %
TIS triggering efficiency $r_{\text{TIS}} = 1.03 \pm 0.03$	1.6 %
PDF parametrisations	1.0 %
Overall relative systematic uncertainty	10.2 %
Fragmentation fractions	7.9 %

5 Summary

A signal of 34.4 ± 6.8 $\bar{B}_s^0 \rightarrow D^0 K^{*0}$ events is observed for the first time. The significance of the background fluctuating to form the B_s^0 signal corresponds to approximately nine standard deviations, as determined from the change in twice the natural logarithm of the likelihood of the fit without signal. Although this significance includes the statistical uncertainty only, the result is unchanged if the small sources of systematic error that affect the yields are included. The branching fraction for this decay is measured relative to that for $\bar{B}^0 \rightarrow D^0 \rho^0$, after correcting for the “non- ρ^0 ” component, to be

$$\frac{\mathcal{B}(\bar{B}_s^0 \rightarrow D^0 K^{*0})}{\mathcal{B}(\bar{B}^0 \rightarrow D^0 \rho^0)} = 1.48 \pm 0.34 \pm 0.15 \pm 0.12, \quad (3)$$

where the first uncertainty is statistical, the second systematic and the third is due to the uncertainty in the hadronisation fraction (f_s/f_d).

The result is in agreement with other measurements of similar ratios and supports the SU(3) breaking observation in colour suppressed $\bar{B}_{(d,s)}^0 \rightarrow D^0 V$ decays. Using $\mathcal{B}(\bar{B}^0 \rightarrow D^0 \rho^0) = (3.2 \pm 0.5) \times 10^{-4}$ [14] for the branching fraction of the normalising decay, a measurement of the $\bar{B}_s^0 \rightarrow D^0 K^{*0}$ branching fraction,

$$\mathcal{B}(\bar{B}_s^0 \rightarrow D^0 K^{*0}) = (4.72 \pm 1.07 \pm 0.48 \pm 0.37 \pm 0.74) \times 10^{-4}, \quad (4)$$

is obtained, where the first uncertainty is statistical, the second systematic, the third due to the uncertainty in the hadronisation fraction (f_s/f_d) and the last is due to the uncertainty of the $\bar{B}^0 \rightarrow D^0 \rho^0$ branching fraction. A future, larger data sample will allow the use of the $\bar{B}^0 \rightarrow D^0 \bar{K}^{*0}$ decay as the normalising channel, which will reduce the systematic uncertainty.

Acknowledgments

We express our gratitude to our colleagues in the CERN accelerator departments for the excellent performance of the LHC. We thank the technical and administrative staff at CERN and at the LHCb institutes, and acknowledge support from the National Agencies: CAPES, CNPq, FAPERJ and FINEP (Brazil); CERN; NSFC (China); CNRS/IN2P3 (France); BMBF, DFG, HGF and MPG (Germany); SFI (Ireland); INFN (Italy); FOM and NWO (Netherlands); SCSR (Poland); ANCS (Romania); MinES of Russia and Rosatom (Russia); MICINN, XuntaGal and GENCAT (Spain); SNSF and SER (Switzerland); NAS Ukraine (Ukraine); STFC (United Kingdom); NSF (USA). We also acknowledge the support received from the ERC under FP7 and the Region Auvergne.

References

- [1] M. Gronau and D. Wyler, “On determining a weak phase from charged B decay asymmetries”, Phys. Lett. B **265** (1991) 172.
- [2] M. Gronau and D. London, “How to determine all the angles of the unitarity triangle from $B_d^0 \rightarrow DK_s^0$ and $B_s^0 \rightarrow D\Phi$ ”, Phys. Lett. B **253** (1991) 483.
- [3] I. Dunietz, “ CP violation with self-tagging B_d modes”, Phys. Lett. B **270** (1991) 75.
- [4] D. Atwood, I. Dunietz and A. Soni, “Enhanced CP Violation with $B \rightarrow KD^0(\bar{D}^0)$ Modes and Extraction of the Cabibbo-Kobayashi-Maskawa Angle γ ”, Phys. Rev. Lett. **78** (1997) 3257, [arXiv:hep-ph/9612433](#).
- [5] D. Atwood, I. Dunietz and A. Soni, “Improved methods for observing CP violation in $B \rightarrow DK$ and measuring the CKM phase γ ”, Phys. Rev. D **63** (2001) 036005, [arXiv:hep-ph/0008090](#).

- [6] A. Giri, Y. Grossman, A. Soffer and J. Zupan, “Determining γ using $B \rightarrow DK$ with multibody D decays”, Phys. Rev. D **68** (2003) 054018, [arXiv:hep-ph/0303187](#).
- [7] P. Colangelo and R. Ferrandes, “Model independent analysis of a class of B_s^0 decay modes”, Phys. Lett. B **627** (2005) 77-81, [hep-ph/0508033](#).
- [8] C.-W. Chiang and E. Senaha, “Updated analysis of two-body charmed B meson decays”, Phys. Rev. D **75** (2007) 074021, [hep-ph/0702007](#).
- [9] The LHCb Collaboration, A. A. Alves Jr *et al.*, “The LHCb detector at the LHC”, JINST **3** (2008) S08005, [iopscience:S08005](#).
- [10] The LHCb Collaboration, “Average f_s/f_d b -hadron production fraction for 7 TeV pp collisions”, [LHCb-CONF-2011-034](#).
- [11] T. Sjöstrand, S. Mrenna and P. Z. Skands, “PYTHIA 6.4 physics and manual”, version 6.422, J. High Energy Phys. **0605** (2006) 026, [arXiv:hep-ph/0603175](#).
- [12] D. J. Lange, “The EvtGen particle decay simulation package”, Nucl. Instrum. Methods A **462** (2001) 152, [EvtGen webpage](#).
- [13] The GEANT4 Collaboration, S. Agostinelli *et al.*, “GEANT4: a simulation toolkit”, version 9.2, Nucl. Instrum. Methods A **506** (2003) 250, [FERMILAB-PUB-03-339](#).
- [14] The Particle Data Group, K. Nakamura *et al.*, “Review of particle physics”, J. Phys. G **37** (2010) 075021, <http://pdg.lbl.gov/>.
- [15] T. Skwarnicki, “A study of the radiative cascade transitions between the Υ' and Υ resonances”, Ph.D. Thesis, [DESY-F31-86-02](#) (1986).
- [16] M. Pivk and F. R. Le Diberder, “SPlot: A statistical tool to unfold data distributions”, Nucl. Instrum. Meth. **A555** (2005) 356, [arXiv:physics/0402083](#).
- [17] The Belle Collaboration, P. Krokovny *et al.*, “Study of $\bar{B}^0 \rightarrow D^0 \pi^+ \pi^-$ decays”, Phys. Rev. D **76** (2007) 012006, [arXiv:hep-ex/0611054](#).
- [18] The BABAR Collaboration, P. del Amo Sanchez *et al.*, “Dalitz plot Analysis $B^0 \rightarrow \bar{D}^0 \pi^+ \pi^-$ ”, [arXiv:hep-ex/10074464](#).